



THE UNIVERSITY
of LIVERPOOL

Reduction in Defect Content of ODS Alloys

November 2003

Report prepared by

J. Ritherdon and A.R. Jones
Department of Engineering,
University of Liverpool,
LIVERPOOL,
L69 3GH
U.K.

under
1DX-SY382V

for

OAK RIDGE NATIONAL LABORATORY,
Oak Ridge, Tennessee 37831

Managed by

UT-BATTELLE, LLC

for the

U.S. DEPARTMENT OF ENERGY,
under contract DE-AC05-00OR22725

This report has been reproduced directly from the best available copy.

Available to DOE and DOE contractors from the Office of Scientific and Technical Information, P.O. Box 62, Oak Ridge, TN 37831; prices available from (865) 576-8401.

Available to the public from the National Technical Information Service, U.S. Department of Commerce, 5285 Port Royal Rd., Springfield, VA 22161.

This report was prepared as an account of work sponsored by an agency of the United States Government. Neither the United States Government nor any agency thereof, nor any of their employees, makes any warranty, expressed or implied, or assumes any legal liability or responsibility for the accuracy, completeness, or usefulness of any information, apparatus, product, or process disclosed, or represents that its use would not infringe privately owned rights. Reference herein to any specific commercial product, process, or service by trade name, trademark, manufacturer, or otherwise, does not necessarily constitute or imply its endorsement, recommendation, or favoring by the United States Government or any agency thereof. The views and opinions of authors expressed herein do not necessarily state or reflect those of the United States Government or any agency thereof.

Contents

Introduction	1
Variability in powder oxidation	1
The effect of powder particle size distribution on canned powder oxidation	1
Variation of oxidation behaviour between different batches of ODS-Fe ₃ Al powder.	2
Minimisation of oxidation	5
Effect of process modifications on powder oxidation	5
Effect of improved vacuum and use of getters on powder oxidation	6
Development of porosity	7
Fluidised bed techniques	10
PM2000/Fe variants	10
PM2000/Al₂O₃ variants	12
Macro-composite materials	13
Hoop grain structures via flow-forming	13
Conclusions	18
References	19

Research sponsored by the U.S. Department of Energy, Fossil Energy Advanced Research Materials Program, DOE/FE AA 15 10 10 0, Work Breakdown Structure Element UL-2.

INTRODUCTION

The work detailed within this report is a continuation of earlier work carried out under contract number 1DX-SY382V.^[1,2,3] The earlier work comprises a literature review of the sources and types of defects found principally in Fe-based ODS alloys as well as experimental work designed to identify defects in the prototype ODS-Fe₃Al alloy, deduce their origins and to recommend methods of defect reduction. The present work is an extension of the experimental work already reported and concentrates on means of reduction of defects already identified rather than the search for new defect types. This report also includes work regarding the manipulation of grain structures via deformation processing and further results gathered during powder separation trials involving the separation of different metallic powders in terms of their differing densities.

The scope and objectives of the present work were laid out in the technical proposal 'Reduction in Defect Content in ODS Alloys – IV'. All the work proposed in the 'Statement of Work' section of the technical proposal has been carried out except for some of that dependent on the acquisition of materials from other sources. However, wherever omissions from the 'Plan of Action' detailed in the 'Statement of Work' have occurred due to lack of suitable materials, other related experimental work has been devised to fill the gaps where possible. All work extra to the 'Statement of Work' falls within the context of an ODS-Fe₃Al alloy of improved overall quality and potential creep performance in the consolidated form. The outturn of the experimental work performed is reported in the following sections.

VARIABILITY IN POWDER OXIDATION

The effect of powder particle size distribution on canned powder oxidation

As-MA ODS-Fe₃Al and PM2000 powders were sieved to prepare size fractions >425 μ m and <75 μ m. These fractions, together with un-sieved as-MA powders were separately, but simultaneously annealed at 1000°C for 1 hour under 10⁻³ mbar in an open ceramic boat. After annealing, the powders were carefully studied using SEM and EDS in cross-section and plan view and the degree of oxidation measured in each case.

After annealing, powder particles of all types and sizes had formed a surface oxide scale, at least on the outermost particles in the annealing crucible. The thicknesses of the scales were measured from cross-sectioned powder particles, but showed no obvious trends associating oxide thickness with particle size. This is shown in Table 1. As seen before, unsieved ODS-Fe₃Al forms a thicker oxide scale than unsieved PM2000.^[3] However, without the benefit of these previous results, it would be difficult to conclude from Table 1 that such a trend exists.

Table 1 Measurement of oxide thicknesses from different alloys and powder particle sizes.

	PMWY2 oxide thickness [μ m]	PMWY3 oxide thickness [μ m]	PM2000 oxide thickness [μ m]
Large fraction	0.68	1.06	0.73
Unsieved	0.72	-	0.53
Small fraction	0.67	-	0.71

The powder particle size ought not to have a significant effect on the thickness of oxide scale that forms over a period as short as 1 hour, such as used in this study. The only parameter that is influenced by particle size is the aluminium reservoir available for the formation of protective alumina scale. Smaller particles would therefore be expected to go into breakaway oxidation sooner than larger particles but over a much greater period of time than covered in this work.^[4]

Although particle size does not appear to have an effect on oxide scale formation, the range of particle sizes within a particular powder appears to affect the distribution of oxidised particles through the depth of a sample of annealed powder. It was found that unsieved powders, with a wide range of particle sizes formed a 'crust' of oxidised particles at the surface of the sample. This crust could be up to 1mm thick on some samples and appeared to protect the powder on the interior of the sample from extensive oxidation. The difference in oxidation levels in the 'crust' and interior can be seen in Figures 1a and 1b.

In powders that had been sieved and therefore covered a narrow range of particles sizes, the degree of oxidation was uniform throughout the powder sample, with significant thicknesses of oxide forming on all particles.

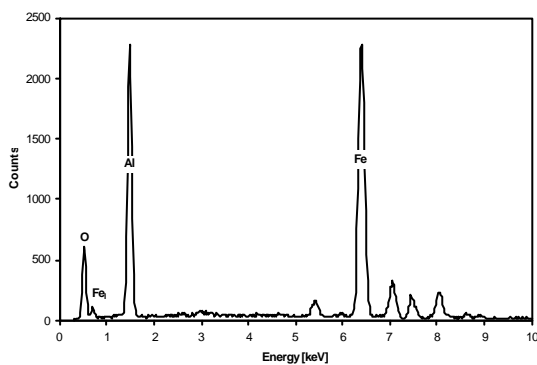


Figure 1a
EDS spectrum from the oxidised powder 'crust'.

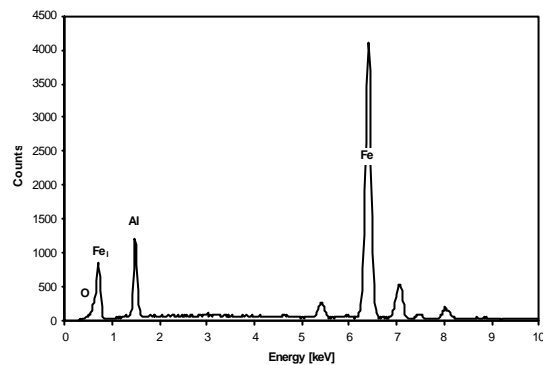


Figure 1b
EDS spectrum from the innermost, protected powder.

The formation of the 'crust' on unsieved powders is attributed to the higher effective tap density possible using powder with a wide range of particles sizes, where smaller particles can pack into interstices between larger powder particles, and so on. Interstices remaining at the onset of annealing are further narrowed by a combination of oxide scale formation and sintering, thus forming a solid crust. This 'crust' was seen to be sufficiently dense to afford shielding from oxidation to further, unoxidized powder deeper within the sample. In sieved powder samples with a narrow range of particle sizes, such thorough packing was not possible and uniform oxidation took place through the whole sample.

Variation of oxidation behaviour between different batches of ODS-Fe₃Al powder.

It has previously been reported that aluminium depleted regions (ADRs) exist within some batches of as-MA ODS-Fe₃Al powder and the size and concentration of these regions varies between powder variants.^[2,3] The greatest differences in ADR content were between ODS-Fe₃Al variants PMWY2 and PMWY3. The oxidation behaviour of these powders has been studied.

Samples of each powder were annealed at 1200°C for 24 hours. In order to accelerate oxidation, the powders were oxidized at atmospheric pressure rather than at the 10^{-3} mbar characteristic of processing atmospheres. After oxidation, the powders were examined by means of SEM and EDS.

As anticipated, after annealing for 24 hours at 1200°C, both PMWY2 and PMWY3 powders exhibited alumina surface layers. However, on the PMWY2 powder, discontinuities in the alumina scale were present in the form of areas of iron oxide. This is shown in Figure 2 where an area of iron oxide can be seen in both the secondary and backscattered electron images together with EDS spectra from the iron oxide and the surrounding alumina scale.

Further samples of powder were cyclically oxidized at 1200°C with 24 hour cycles in ambient laboratory air. After each cycle, the samples were weighed and their masses plotted against time in order to monitor the progression of oxidation.

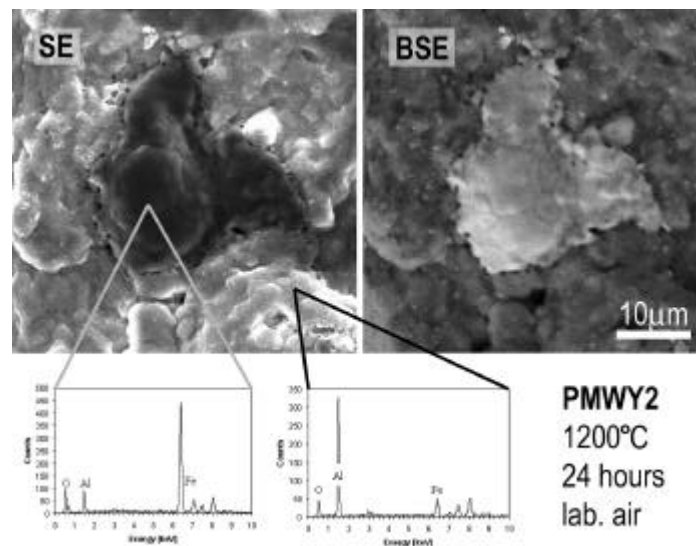


Figure 2 Iron oxide region found within the alumina scale on an oxidized PMWY2 ODS- Fe_3Al powder particle.

The mass gain data collected during cyclic oxidation of the powders can be seen in Figure 3. Both powders show an initial rapid increase in mass and then the mass increase slows to a steady level, slightly higher in powder PMWY2. After 120 hours, the mass increase of the PMWY2 powder accelerated. This increased rate coincided with the formation of regions of a black oxide on increasing numbers of the PMWY2 particles. Powder PMWY3 did not show such an increase in mass gain rate until after 250 hours and, even then, the mass gain rate was not as high as that seen in PMWY2. Again, the rate increase coincided with the formation of a black oxide.

The surface area to volume of the two powder batches was measured using stereological methods. The values calculated for PMWY2 and PMWY3 were 1.60 and 1.11cm^{-1} respectively.

The weight fractions of fine material entrained in fissures and adhered to the surface of the two powder types was estimated by ultrasonically cleaning the powders in ethanol in an attempt to dislodge as much of the finer material as possible. The fine sediment was collected

and weighed and the weight fractions of fines for PMWY2 and PMWY3 were 0.14 and 0.10wt% respectively.

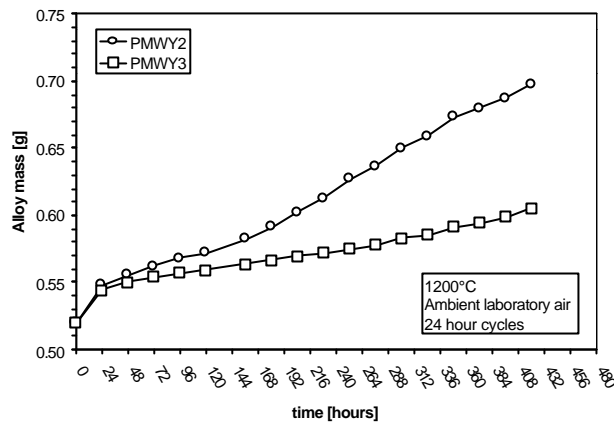


Figure 3 Mass gain of powders PMWY2 and PMWY3 during cyclic oxidation.

The average thickness of the scale formed on the powders during annealing was measured using cross-sectional samples of powder particles and SEM. The increase in scale thickness with time is shown in Figure 4.

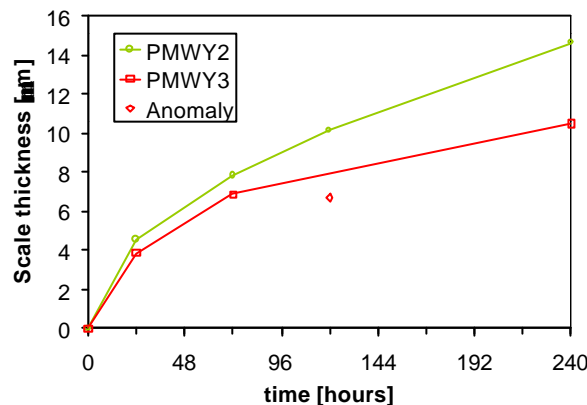


Figure 4

Increases in scale thickness on PMWY2 and PMWY3 with oxidation time at 1200°C

The formation of similar alumina scales over the majority of powder particles from both of the powder variants studied would be expected as the alloys are of practically the same composition. This is what was observed in the powders oxidised in this work although the presence of substantial islands of iron oxide within the alumina scale formed on variant PMWY2 suggests that differences do exist in oxidation behaviour.

It is possible that the iron oxide islands are associated with ADRs that intersect the particle surface. However, this could not be observed in cross sectional samples. It is more likely that the iron oxide occurs where fine material has gone into breakaway oxidation because of its low mass and aluminium reservoir. PMWY2 contained a greater fraction of fines and this breakaway effect would therefore be expected to be prevalent in batch PMWY2.

The larger surface area/volume ratio for PMWY2 would also be expected to increase weight gain rate during oxidation. There is no reason to believe that this is not the case but the estimated increase in weight gain rate that would be associated with the surface area ratios measured falls well short of the differences in weight gain observed.

In fact, the most likely explanation for the higher weight gain seen in batch PMWY2 is simply that the oxide scale thickened more rapidly, increasing the powder mass and decreasing the aluminium reservoir so that breakaway oxidation occurred earlier. The scale thickness vs. time graph shown in Figure 4 bear a strong resemblance in terms of relative proportions to the mass gain graphs. The small reduction in aluminium content of PMWY2 attributed to the presence of ADRs cannot account for the more rapid onset of breakaway oxidation seen in PMWY2. Indeed, it has been estimated by modelling the decrease in aluminium with oxidation time that ADRs would be expected to foreshorten the oxidation lifetime of ODS-Fe₃Al by only 3.6%; insignificant compared to the 53% reduction in lifetime actually observed.

The ADRs do, however, represent areas of the alloy depleted not only in aluminium, but also depleted in yttria-based compounds essential for good oxide adhesion as well as alloy strength.^[5] The reduced level of aluminium in such particles may hinder alumina formation and would promote the formation of iron and possibly chromium oxides to some extent, particularly in the early stages of oxidation before diffusion induces chemical homogeneity. The resulting defective scales appear to thicken more quickly, fed by the easy ingress of atmospheric oxygen to the underlying alloy. The lack of yttria in ADRs would also contribute to earlier, local decohesion of protective scale and accelerate the tendency towards breakaway oxidation. This effect would be more obvious in longer-term oxidation than the 24 hour oxidation illustrated in Figure 2, and may be responsible for the early breakaway oxidation of variant PMWY2 seen in the mass gain data in Figure 3. Here the adhesion and homogeneity of the protective scale could be compromised by areas lacking in yttria dispersoid, resulting in an oxidation lifetime only half that of PMWY3. Onset of breakaway oxidation could be seen to be quite gradual compared to mass gain data typical of single coupons of ODS alloys. This is attributed to the fact that a broad population of particles was oxidised in the same crucible during the experiment. Each particle behaved slightly differently and the onset of breakaway oxidation was distributed over a period of time as a cumulative effect of individual powder particles going into breakaway one by one.

MINIMISATION OF OXIDATION

Effect of process modifications on powder oxidation

As-MA PM2000 powder was compacted in a cylindrical die (Ø10mm x 6mm) by simple uniaxial compression to a pressure of 635 MPa. To simulate canning, the powder, still contained in its die, was annealed at 1000°C for 1 hour under a vacuum of 10⁻³ mbar. After annealing, the compressive strength of the resulting powder was measured.

In a further trial, as-MA ODS-Fe₃Al and PM2000 were both compacted and annealed as above, but with the inclusion of two hydrogen purges of the vacuum system prior to evacuation to 10⁻³ mbar. Due to significant shrinkage during sintering, the resulting pellets were severely cracked and compressive strengths were estimated from hardness measurements taken from the pellet fragments.

The effects of hydrogen purging on ODS-Fe₃Al and PM2000 powder charges and the effect of cold compaction of ODS-Fe₃Al powder prior to annealing on powder oxidation and subsequent sintering efficiency have already been reported.^[3] Figure 5 shows these data alongside the new data on the effects of cold compaction of PM2000 powder and the effect of combining hydrogen purging with cold compaction for both ODS-Fe₃Al and PM2000.

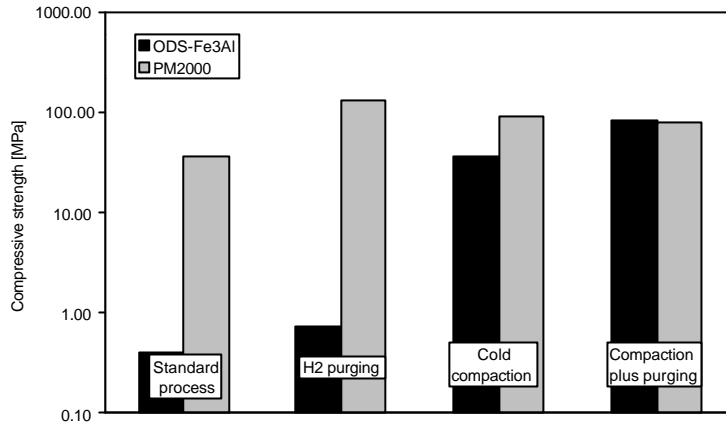


Figure 5 The effect of process modifications on the sintered strength of ODS-Fe₃Al and PM2000 powders.

It can be seen that cold compaction of the alloy powder prior to annealing produced a dramatic improvement in sintered strength. Whereas hydrogen purging alone produced the largest enhancement in sintered strength in PM2000 powder, cold compaction increased sintered strength in ODS-Fe₃Al powder by a factor of 89 as opposed to the factor of ~3 increase seen with PM2000 powder. It is believed that this is due to more rapid oxidation in ODS-Fe₃Al powder than PM2000 and, therefore, that the most effective way to reduce oxidation during consolidation is to minimise the powder free surface area by use of processes such as cold compaction.^[3,6]

The two techniques can be seen to be highly effective but in an alloy specific way. It could have been expected, therefore, that the combination of the two techniques would not yield significant further improvements on the application of the individual techniques. In the case of PM2000 powder, this was indeed the case, with no obvious additional benefit (within experimental error) gained by combining purging and compaction. However, a further improvement in sinter strength was possible for the ODS-Fe₃Al alloy: a sintered pellet produced by a combination of hydrogen purging and cold compaction had a compressive strength a factor 203 times higher than that produced by straightforward vacuum annealing. The ODS-Fe₃Al pellet was, in fact, of similar strength to a similarly processed PM2000 pellet whereas after straightforward annealing, the PM2000 pellet was a factor of 90 times stronger. It would appear that a combination of cold compaction and hydrogen purging can significantly reduce the oxidation of densely packed ODS-Fe₃Al during annealing.^[7]

Effect of improved vacuum and use of getters on powder oxidation

It has been shown that increasing the pressure i.e. degrading the vacuum during powder annealing has a marked effect on powder oxidation. When the pressure was increased from 10⁻³ to 10⁻²mbar during annealing of PM2000 powder, oxidation of the surface of the powder particles took place to such an extent that the fragmented oxide decorated prior particle surfaces in the sintered compact.^[7] A cross section of the sintered PM2000 is shown in Fig 6.

A reduction of pressure i.e. improved vacuum appears to give a reduction in oxidation. However, as oxidation is so slight at the standard pressure of 10⁻³mbar, the reduction achieved by reducing the pressure to 10⁻⁴mbar, for example, is barely measurable. In commercial processes, vacuum pumping is achieved by means of rotary pumps and it is difficult to achieve vacuums of 10⁻³mbar even after lengthy pumping. In order to achieve higher

vacuums new pump technology would need to be employed and, even then, very little improvement in oxidation behaviour could be expected. It is therefore deemed impractical to prescribe a production route that includes higher vacuum annealing than is presently employed.

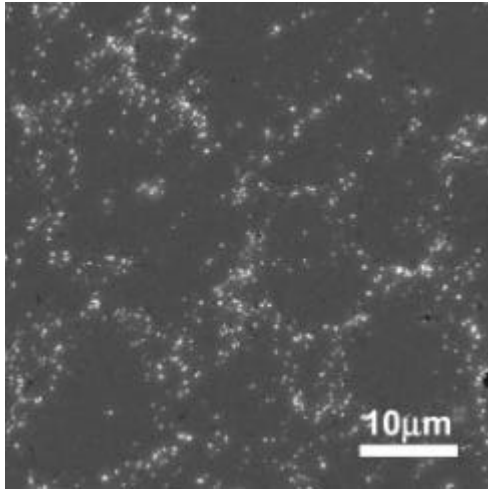


Figure 6
SEM cross-sectional image of cold compacted FeCrAl annealed at 1000°C for 1 hour under 10^{-2} mbar. Entrained oxide particles can be seen delineating erstwhile powder particles.

An alternative method for reducing the partial pressures of oxidizing gases in the vacuum is the use of getters. The use of titanium and zirconium getters within cans of powder has been studied to ascertain whether or not such getters can reduce powder oxidation during high temperature annealing.

So far, experiments have shown no reduction of powder oxidation using these getters in their present form of foil and helical wire linings to the can.

It is believed that actual reduction of the alumina scale, although thermodynamically possible, is not feasible under these conditions where the getter is remote from much of the powder charge. Although getters should reduce the partial pressure of oxygen in the can, it is believed that by the time this had taken place, powder oxidation has already occurred.

DEVELOPMENT OF POROSITY

Porosity is seen to develop in the alloy PM2000 after protracted annealing at high temperatures.^[8] In order to compare this behaviour with that of ODS-Fe₃Al, samples of PMWY2 were annealing in air at 1300°C for 2016 hours (12 weeks) and were examined after 672, 1344 and 2016 hours annealing for signs of porosity. These conditions would be ample to cause porosity in PM2000. The samples were taken from PMWY2 which had been extruded at an extrusion ratio of 9:1 and from PMWY2 extruded at 16:1.

Even after 2016 hours annealing, no porosity was observed except that caused by the drop-out of particles and intrusions. A section through an intrusion is shown in Fig 7 and the pore left when such an intrusion drops out of the sample is shown in Fig 8. From Fig 8 it can clearly be seen that the inside surface of the pore is decorated with oxide particles. Two possibilities for the origin of these particles are that they i) are the oxide debris that was present before consolidation and that isolated the intrusion from the bulk or ii) they are the result of the formation of a pore that has accumulated non-metallic debris on its inner surface as the pore has grown and the metal receded. As the pore matches intrusions in size, and oxide debris has been observed around intact intrusions, it is believed, at this stage, that the pore shown in Fig 8 and similar pores are formed by the dropout of intrusions.

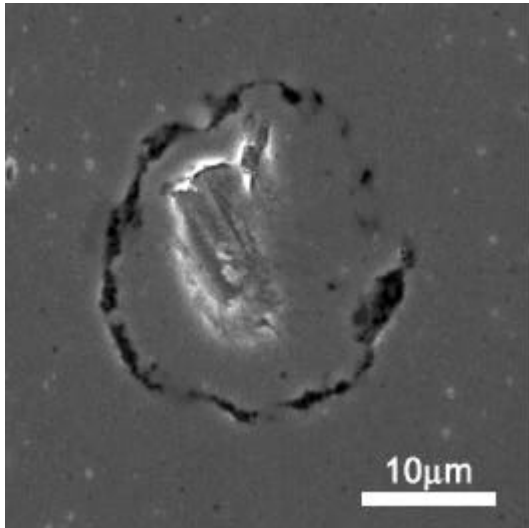


Figure 7
A section through an intrusion in ODS- Fe_3Al annealed at 1300°C for 673 hours.

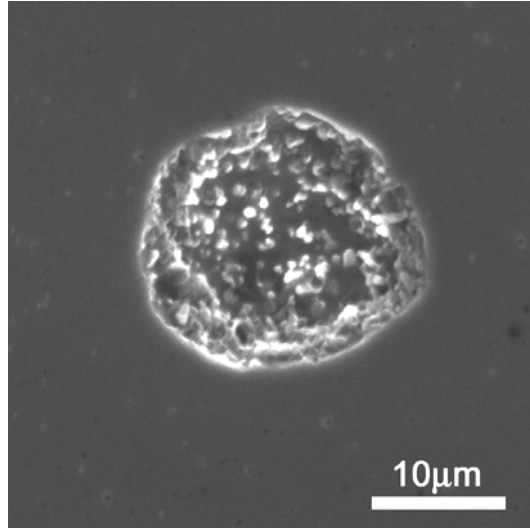


Figure 8
A pore resulting from the drop-out of an intrusion in ODS- Fe_3Al annealed at 1300°C for 672 hours.

As seen before, the ODS- Fe_3Al material extruded at an extrusion ratio of 16:1 contains a large amount of particulate matter comprising mainly alumina (see Fig 9).^[9] Such oxide particles were present in high concentrations particularly in the 16:1 ODS- Fe_3Al used in the annealing tests and the coarseness of the particles seemed to increase slightly with annealing time. However, overall the two variants tend to behave similarly with any differences attributable to the differences present before annealing e.g. the high alumina content of the 16:1 variant.

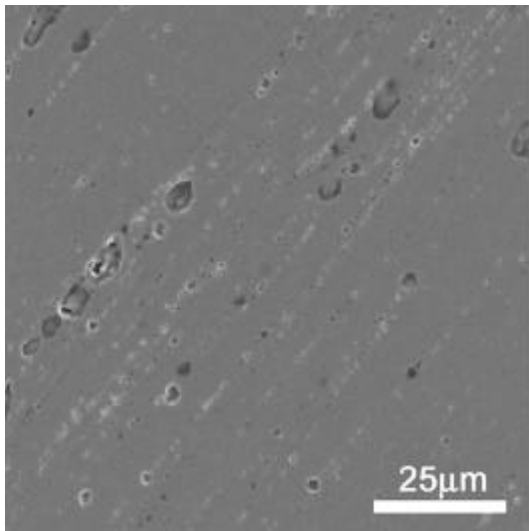


Figure 9
High concentrations of oxide particles and pores caused by particle drop-out in ODS- Fe_3Al (extruded at 16:1) annealed at 1300°C for 672 hours.

It was observed that intrusions became gradually more obvious with annealing time. It is not clear whether this is due to ripening of the oxide particles which surround intrusions or to the formation of pores and voids around the intrusions at the intrusion/bulk interface. Both voids and oxide particles were visible at all stages in the annealing and both were perceived to grow with time at temperature although no measurements were taken.

Particles of a new phase formed on annealing which gradually grew with annealing time but stabilised at around $5\mu\text{m}$ as seen in Fig. 10a. SEM-EDS analysis indicated that they are aluminium/iron nitrides (Fig. 10b).

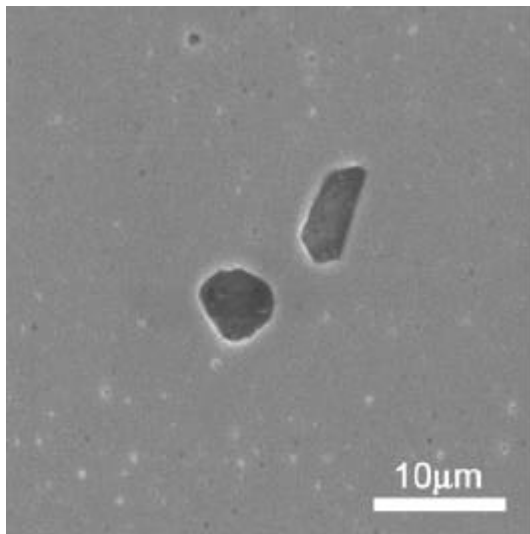


Figure 10a
Particles which formed in ODS-Fe₃Al after annealing at 1300°C for 673 hours.

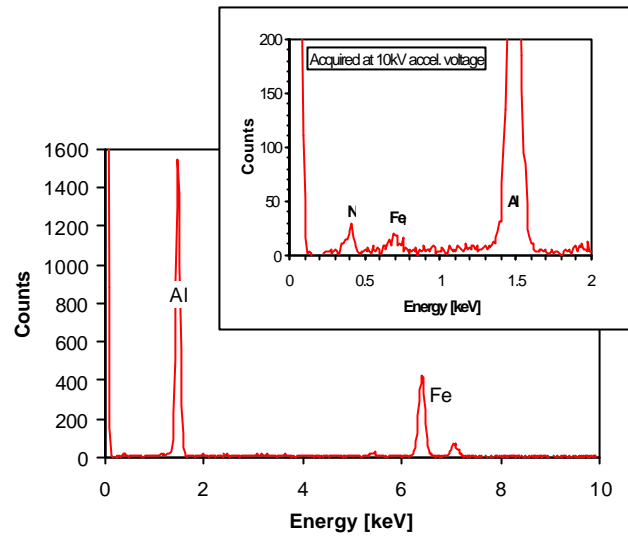


Figure 10b
EDS spectrum taken from particles similar to those in Figure 10a after annealing at 1300°C for 2016 hours.

It is surprising (from comparison with other FeCrAl alloys) that these nitrides form so early during annealing. Nitride formation in FeCrAl alloys has previously been seen only after aluminium depletion to critical oxidation levels has occurred after protracted oxidation. As can be seen in Fig 11, although microprobe analysis shows that some aluminium depletion has taken place during annealing, levels are still many times higher than typical critical levels even after 2016 hours.

However, such nitride formation is linked to the porous and defective oxides formed with low aluminium levels rather than to the low aluminium levels themselves. It is suggested that the oxide scale formed on the ODS-Fe₃Al alloys is slightly porous and not altogether protective, allowing atmospheric components to pass through to the alloy substrate during annealing, leading to the formation of nitrides and the possible coarsening of oxide particles.

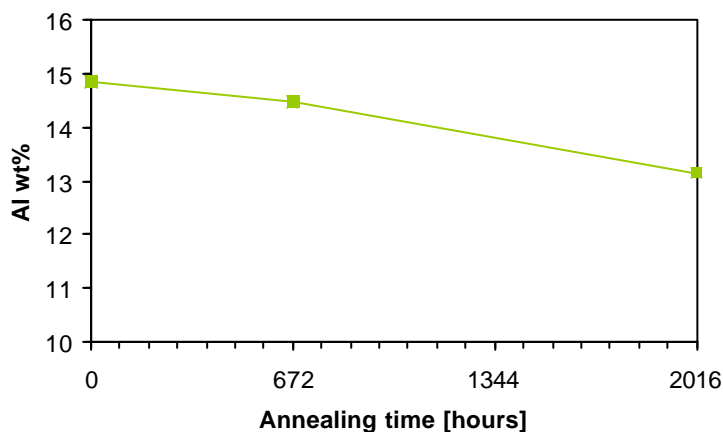


Figure 11
Graph showing the degree of aluminium depletion during the annealing of ODS-Fe₃Al at 1300°C.

FLUIDISED BED TECHNIQUES

A major aspect of this work was to assess whether the fluidised bed separation technique might be applied commercially, particularly in the production of MA metallic powders such as the MA ODS-FeCrAl alloys. In an attempt to simulate a commercial situation, ~8kg of gas-atomised Fe₃Al powder (\bar{n} =6.53 g.cm⁻³, mean diameter 83 μ m) was seeded with ~0.16kg (~2wt.%) of ODS-Fe₃Al sievings (\bar{n} =6.5-6.6 g.cm⁻³, mean diameter >400 μ m) known to contain aluminium-depleted inhomogeneities. Separation by density was attempted as might be used in a commercial production process. The separation process was run both with and without internal baffles in order to assess the effect of the baffles on segregation efficiency.

Separation of the defective ODS-Fe₃Al seed powder from the gas-atomised Fe₃Al powder was successfully achieved with the seed powder segregating to the bottom of the bed as shown in Figure 12. Here 98.5mass% of the seed powder was concentrated in the bottom 6mm of the bed. However, the seed particles are of different morphology to the bulk powder and, more importantly, are larger and more massive. All else being equal, larger particles tend to sink in a fluidised bed so it was necessary to ascertain, rather than simply whether separation was feasible, the degree to which the sinking effect could be influenced or 'tuned' by the inclusion of vibrating baffles. It was found that removal of the vibrating internal baffles appeared to have only a marginal effect on the separation characteristics of the bed. This is illustrated in Figure 13 where the segregation profile of the seed powder is almost identical to that seen in Figure 12 with 95.0mass% concentrated in the bottom 6mm of the bed. Here only the distribution of the coarse particles is considered relevant. The higher mass% values seen in the bed without baffles are a reflection of differences in the starting concentration of coarse particles and not of segregation efficiency.

It is believed that the effect of particle size is dominant in this system since particle size varies by a factor greater than five while the densities differ only a few percent. However, despite the large difference in particle size and the strong segregation that it elicits, some improvement in the segregation characteristics may be achieved by the inclusion of vibrating baffles.

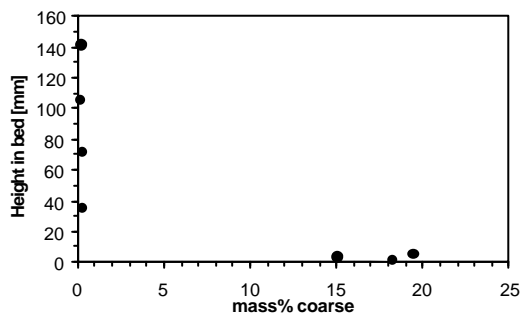


Figure 12
Concentration of coarse seed particles at different heights in a fluidised bed with no internal baffles.

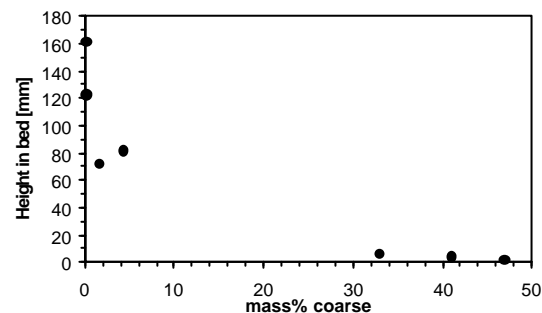


Figure 13
Concentration of coarse seed particles at different heights in a fluidised bed with internal baffles.

PM2000/Fe VARIANTS

A variant of PM2000 rod containing up to 1 wt.% of pure Fe powder was produced by Plansee GmbH, Lechbruck, Germany. The Fe powder was chosen to introduce ODS-free

regions into the PM2000 in order to investigate any effects that this might have on the recrystallisation behaviour of the alloy.

The presence of fine-grained stringers of recrystallised material has previously been observed in ODS-Fe₃Al.^[1,10]

A major contributory factor credited in their formation was the presence of ODS-free regions within the ODS-Fe₃Al due to the entrainment of fragments of mill attritor in the alloy powder during mechanical alloying. A lack of oxide dispersoid might be expected to enable recrystallisation to occur and progress much more readily locally than usually seen in ODS alloys. This was found to be the case and stringers of recrystallised material have been found in consolidate, as-extruded ODS-Fe₃Al which had undergone no secondary recrystallisation annealing. A transverse section of such a stringer is shown in Figure 14 with recrystallised grains arrowed.

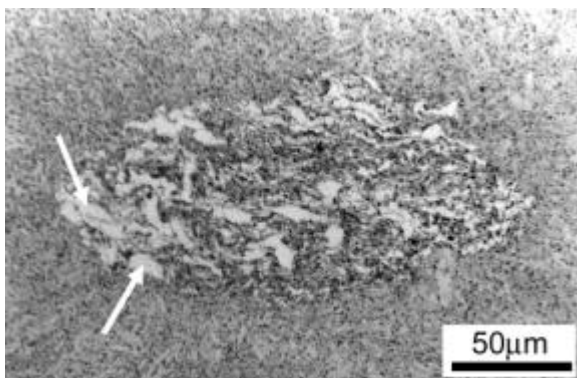


Figure 14
Stringer of recrystallised material in as-extruded ODS-Fe₃Al (PMWY2).

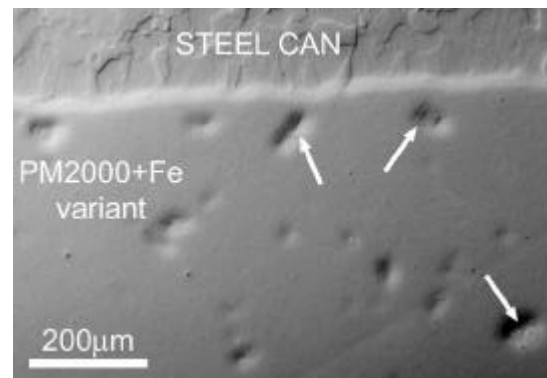


Figure 15
Recrystallised regions in the as-extruded PM2000+Fe variant.

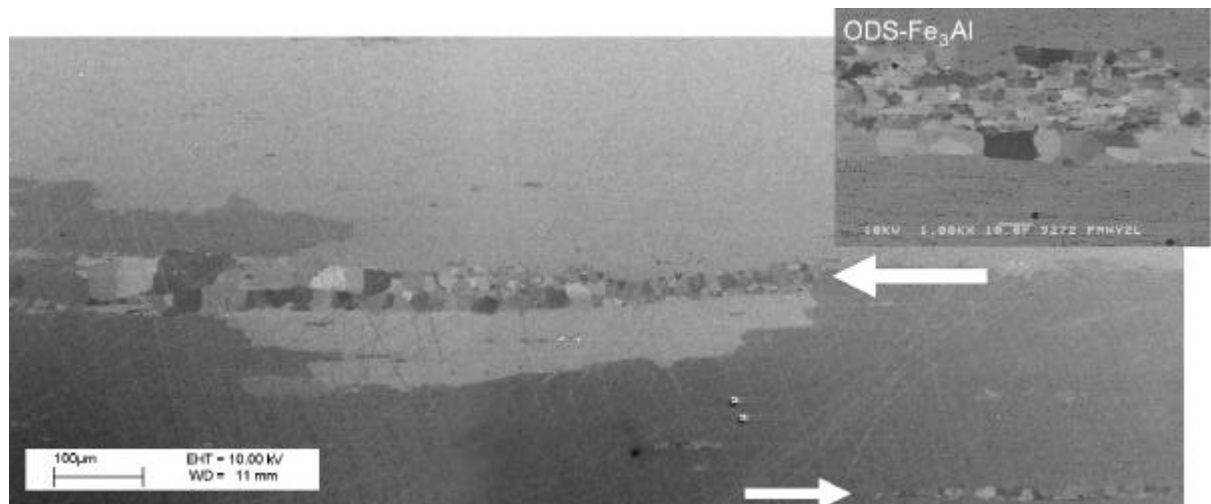


Figure 16
FEG-SEM channelling contrast image of stringers of fine grains (arrowed) in secondary recrystallised PM2000+Fe variant compared to similar fine-grained stringers found in secondary recrystallised ODS-Fe₃Al (inset). Longitudinal sections.

It was suspected that the addition of Fe powder to PM2000 might produce similar recrystallisation effects. Early findings suggest that this is the case. Figure 15 shows a transverse section of the as-extruded PM2000 variant where, already, certain areas have

recrystallised (arrowed). The recrystallised regions are much more uniform in size, morphology and distribution than those seen in ODS-Fe₃Al, presumably because they originate from carefully controlled additions of sized powder rather than from random fragments of mill attritor. The similarities between the fine-grained stringers found in the prototype ODS-Fe₃Al and those found in the PM2000 variant are clear in the micrographs in Figure 16. Here a transverse section of the PM2000 variant after annealing at 1380°C for 1 hour is compared to a transverse section of ODS-Fe₃Al after secondary recrystallisation annealing (inset). The implication is that the fine-grained stringers in ODS-Fe₃Al are introduced by ODS-free regions and this effect can be repeated in a different alloy, PM2000, by controlled introduction of ODS-free regions. The influence of these ODS free regions on the more macroscopic recrystallisation behaviour of these alloys is the subject of continuing study.

PM2000/Al₂O₃ VARIANTS

Alumina powder of MPD 0.86µm was added to PM2000 powder prior to consolidation at a concentration of 1wt.%. The recrystallised grain structure was essentially similar to that seen in the PM2000/Fe variant. However, no recrystallised stringers were found after short annealing times. The alumina particle distribution was clearly visible by optical microscopy and alumina-free regions exist throughout the alloy, presumably corresponding to erstwhile PM2000 powder particles. After 1 hour at 1380°C, any small grains tended to exist within these alumina-free regions and appeared to have been constrained by the alumina particles at the periphery of the region.

In order to see whether or not these alumina particles are capable of triggering early recrystallisation as described in the literature ^[11], samples were bent to an inner diameter of 10mm and then annealed at 1380°C for 1 hour. The bending is intended to give a variation in strain across the sample thickness in the hope that a critical strain necessary to trigger early recrystallisation could be found. To date, particle-triggered recrystallisation has not been achieved and further trials using coarser (MPD 10µm) alumina powder are underway.

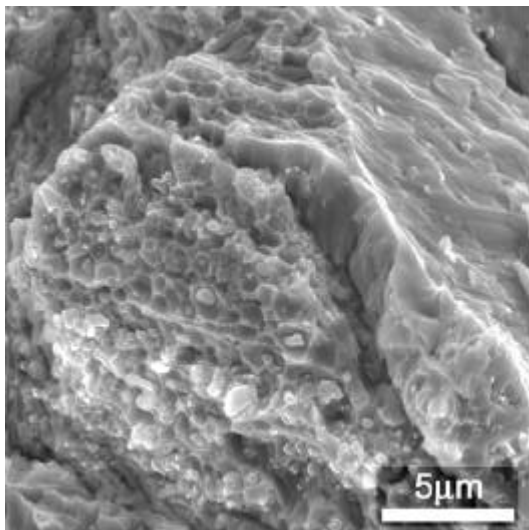


Figure 17

The fracture surface of the PM2000/Al₂O₃ variant which cracked during cold rolling. The crack largely followed the surfaces of the Al₂O₃ particles.

The addition of alumina particles was, however, seen to have a dramatic effect on the variant's mechanical properties, in particular its ductility. The PM2000/Al₂O₃ was seen to fracture during cold rolling after only around 10% deformation whereas the PM2000/Fe variant underwent 25% cold deformation without cracking. SEM examination of the PM2000/Al₂O₃ fracture surface showed that the alumina particles had surrounded the

PM2000 particles prior to consolidation and then formed stringers of particles during extrusion. These stringers provided paths for rapid crack propagation along the particle/alloy interfaces as seen in Figure 17

MACRO-COMPOSITE MATERIALS

During production of the PM2000/variants, the mild steel can used to hold the powders during consolidation were not removed from the extruded rod. Instead, they were left intact and annealed with the variants to investigate whether or not the recrystallisation behaviour of the mild steel would affect the recrystallisation behaviour of the PM2000. Samples were cut from the extruded variant rods and annealed at 1380°C for 1 hour.

In the PM2000/Fe variant no interaction was observed between the recrystallisation of the mild steel and the PM2000 even though the interface between them appeared to be clean and thoroughly welded as shown in Figure 18. It is thought that because the recrystallisation of the mild steel would occur much more readily than that of the PM2000, the recrystallisation processes of the two metals must occur so disparately as to be 'invisible' to each other and therefore do not interact. The effect is believed to be similar to that seen in ODS-Fe₃Al and the PM2000/Fe variant alloy where stringers of ODS-free materials recrystallise readily but do not appear to interact with the surrounding alloy.

The PM2000/Al₂O₃ variant similarly showed no interaction between the recrystallisation processes of the mild steel and the PM2000. Again it is thought that this is due to widely disparate recrystallisation times and temperatures. However, in the case of the PM2000/Al₂O₃ variant, the steel/PM2000 interface was heavily decorated with Al₂O₃ particles which would be expected to hinder boundary migration in any case. This interface can be seen in Figure 19.

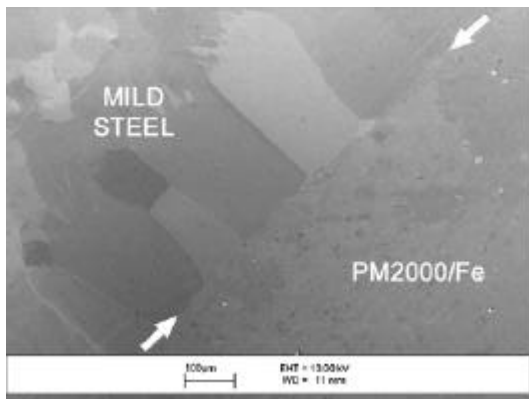


Figure 18
The interface between the consolidated PM2000/Fe variant and its mild steel can.

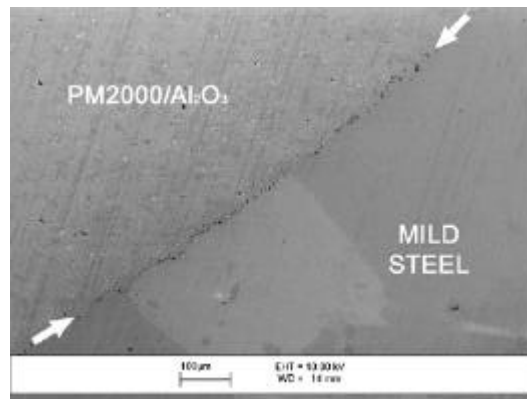


Figure 19
The interface between the consolidated PM2000/Al₂O₃ variant and its mild steel can. The alumina particles adorning the interface can be clearly seen.

HOOP GRAIN STRUCTURES VIA FLOW-FORMING

Extruded PM2000 tubes were flow formed at elevated temperature (600-700°C) and to various levels of strain then subject to secondary recrystallisation anneals. Optical micrographs of three such tubes are shown in Figure 20. The tube microstructure bears a

clear relationship to the paths of the flow forming rollers with grains contained within the helical tracks left by the rollers after processing. Although the grains in all three tubes demonstrated similar degrees of axial constraint, their extent in the hoop direction was less uniform. At lower levels of deformation the grains did not extend far in the hoop direction and tended to be rather “blocky” in appearance as seen in tube W4 (74% deformation). In tube W7 (86% deformation), on the other hand, grains developed to a much greater extent in the tube hoop direction, resulting in grains with a very high GAR orientated parallel to the hoop direction. Due to the promising nature of the grain structure obtained with tube W7, further investigations were performed to determine the influence of flow forming on the development of desirable hoop grain structures in this tube.

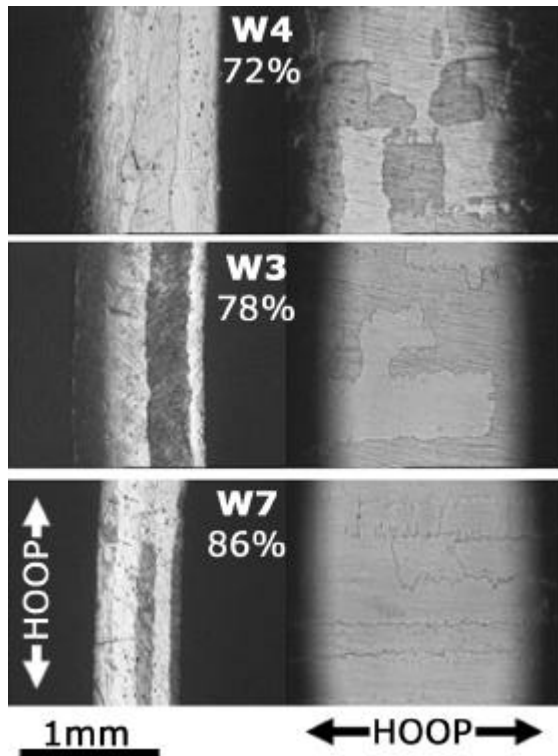


Figure 20

Optical micrographs of transverse sections and plan views of secondary recrystallised, warm flow formed tubes showing the effect of different levels of deformation on grain size and morphology.

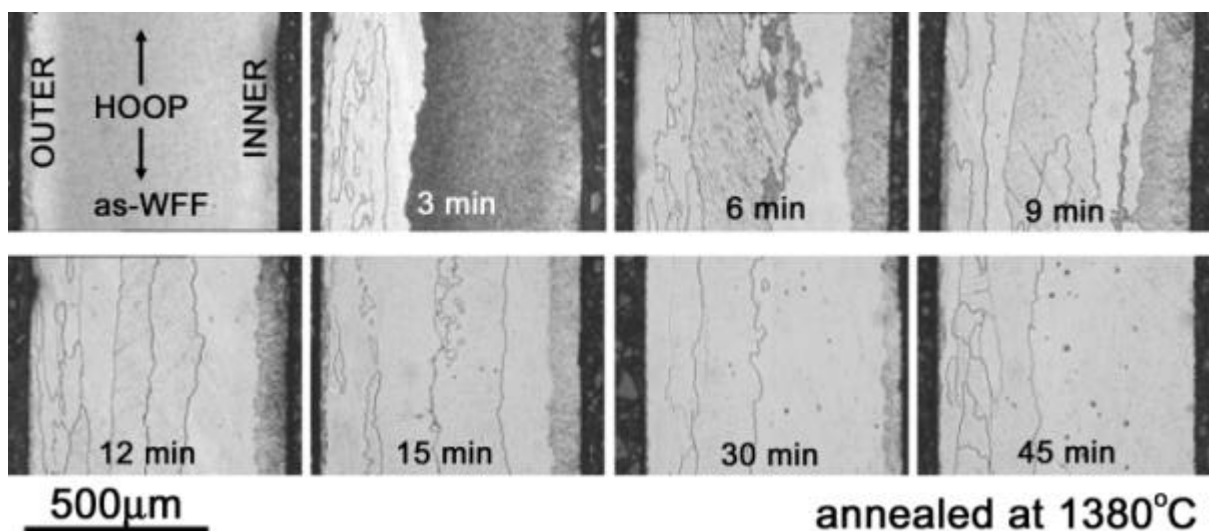


Figure 21

Optical micrographs of transverse sections of tube W7 annealed at 1380°C for different times. The progression of secondary recrystallisation can be seen through the tube wall thickness.

Samples cut from tube W7 were annealed at 1380°C to effect secondary recrystallisation. A range of annealing times was chosen so that the progression of the secondary recrystallisation process could be observed. Optical micrographs of transverse sections of tube W7 annealed for progressively longer times are shown in Figure 21. It can be seen that the majority (~80%) of the tube had recrystallised after 9 minutes annealing and that recrystallisation commenced towards the tube outer surface and progressed rapidly inwards. However, subsequently, the rate of recrystallisation dropped dramatically and only after 45 minutes did the sample appear to be wholly secondary recrystallised. This is believed to be directly linked to the single-sided nature of the deformation applied during flow forming where plastic strain was highest at the outer surface and decreased towards the inner surface of the tube which was supported on a mandrel.

In the earliest stages of recrystallisation, after a nominal 15 second exposure at 1380°C, it was noted that recrystallisation initiated just below the tube outer surface at a depth of around 100µm, as can be seen in Figure 22. From this position, recrystallisation spread both outwards and inwards, reaching the outer surface within the first minute at temperature. The reasons why recrystallisation does not initiate at the outer surface of the tube are the subject of continuing investigation.

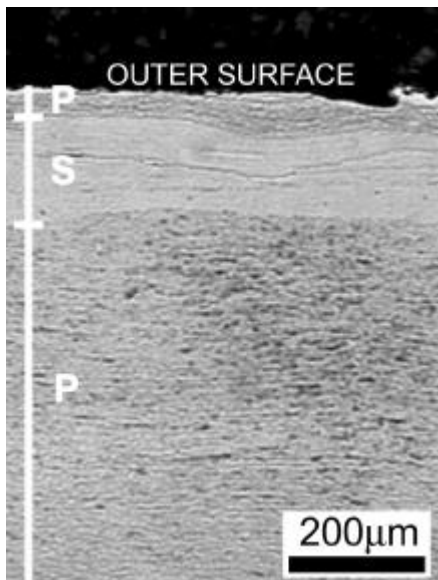


Figure 22

Optical micrograph of a longitudinal section of tube W7 annealed for 15 seconds at 1380°C, showing that secondary recrystallisation originates from a layer just below the outer surface to spread outwards and inwards with time at temperature.

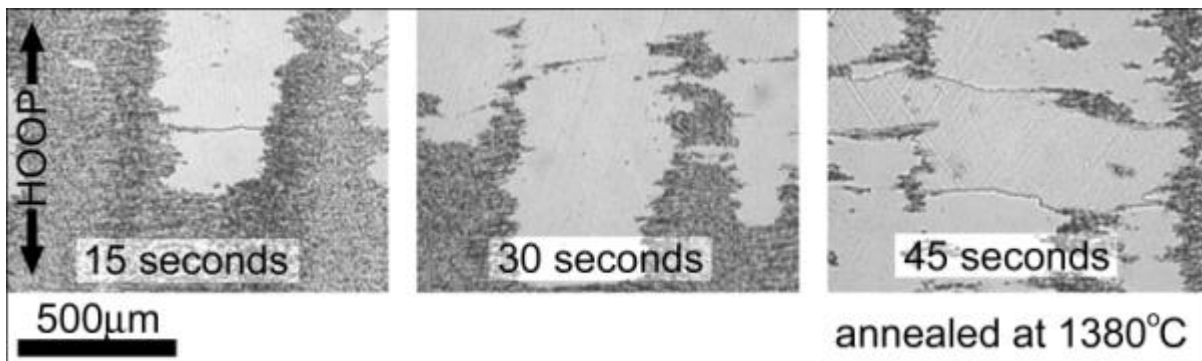


Figure 23

Optical micrographs of plan views of shallow taper sections of tube W7. The uneven secondary recrystallising front can be seen to be spreading downwards towards the outer surface of the tube more rapidly in some areas than in others.

Shallow taper sections of the outer surface of tube W7 were prepared so that the recrystallisation behaviour of the outer 100-200µm could be more easily observed. The progression of the secondary recrystallising front can be seen as it approached the outer surface during the first 45 seconds of annealing in Figure 23. The recrystallising front was not planar and did not intersect the tube outer surface evenly. Rather, it advanced more rapidly directly beneath the centres of the tracks left by the flow forming rollers and reached the outer surface first at these track centres. This resulted in the “comb-shaped” distribution of the primary recrystallised alloy seen in the taper sections, as primary recrystallised material extended more deeply into the tube wall below the edges of the roller tracks. The alloy directly below the track edges appeared to be less prone to secondary recrystallisation than the alloy below the track centres and forms weak barriers to the axial spread of secondary recrystallised grains at the tube surface. Secondary recrystallisation appeared subject to no such barriers in the hoop direction and grains were, therefore, free to develop a substantial hoop-orientated GAR.

The result of all these effects is that the final secondary recrystallised grain structure varied considerably through the tube wall with four (arbitrary) regions of distinct grain morphology and size. The extent of these regions is shown schematically in Figure 24 and the morphology of the grains is described in Table 2. Except for the outer hoop-orientated structure, the grains in the rest of the tube were found to be elongated, with major axis parallel to the tube axial direction. The grain size was found to increase markedly towards the inner surface of the tube, which implied much more limited nucleation of recrystallisation away from the tube outer surface. Moreover, the GAR changed with increasing grain size becoming more equiaxed in the axial-hoop plane. As mentioned, the flow forming process applies rolling forces from the outside of the tube giving a deformation gradient through the tube wall with high deformation and high nucleation rates at the tube outer surface and lower total deformation and nucleation rates at the tube inner wall.

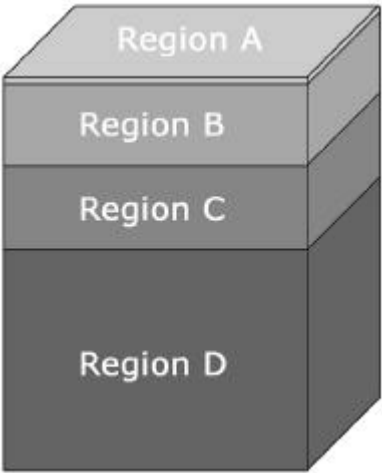


Figure 24
Schematic diagram showing the distribution of the four regions of different grain size and shape through the tube wall.

Table 2

	Region depth [mm]	Grain sizes [mm]		
		Axial	Radial	Hoop
Region A	10	600	10	50000
Region B	140	650	90	100
Region C	150	2500	150	1500
Region D	400	10000	350	7500

The shallowness of the outer layer of hoop-orientated grains is linked to the difference in recrystallisation kinetics seen at roller track centres and edges. It is likely, therefore, that the depth of deformation during forming *per se* is not sufficient to produce such grain structures. The levels or types of deformation at the centres and edges of the tracks left by the flow forming rollers was thought of at least equal significance and worthy of further investigation.

With this in mind, Electron BackScattered Diffraction (EBSD) data was collected from different areas of a taper sectioned sample of tube W7 using a CamScan X500 Crystal Probe. The sample had been annealed for (nominally) 15 seconds at 1380°C. Data were collected from primary recrystallised material at the outer surface of the tube from positions below both the roller track centres and edges. Data were collected from immediately below the tube outer surface, from points deeper into the tube wall, and also from positions below several separate roller tracks, to check that any effects were periodic and associated with roller tracks and not simply random fluctuations. $\langle 100 \rangle$ pole figures and misorientation angle distribution histograms from points at the track centre and track edge and just below the tube outer surface are shown in Figure 25.

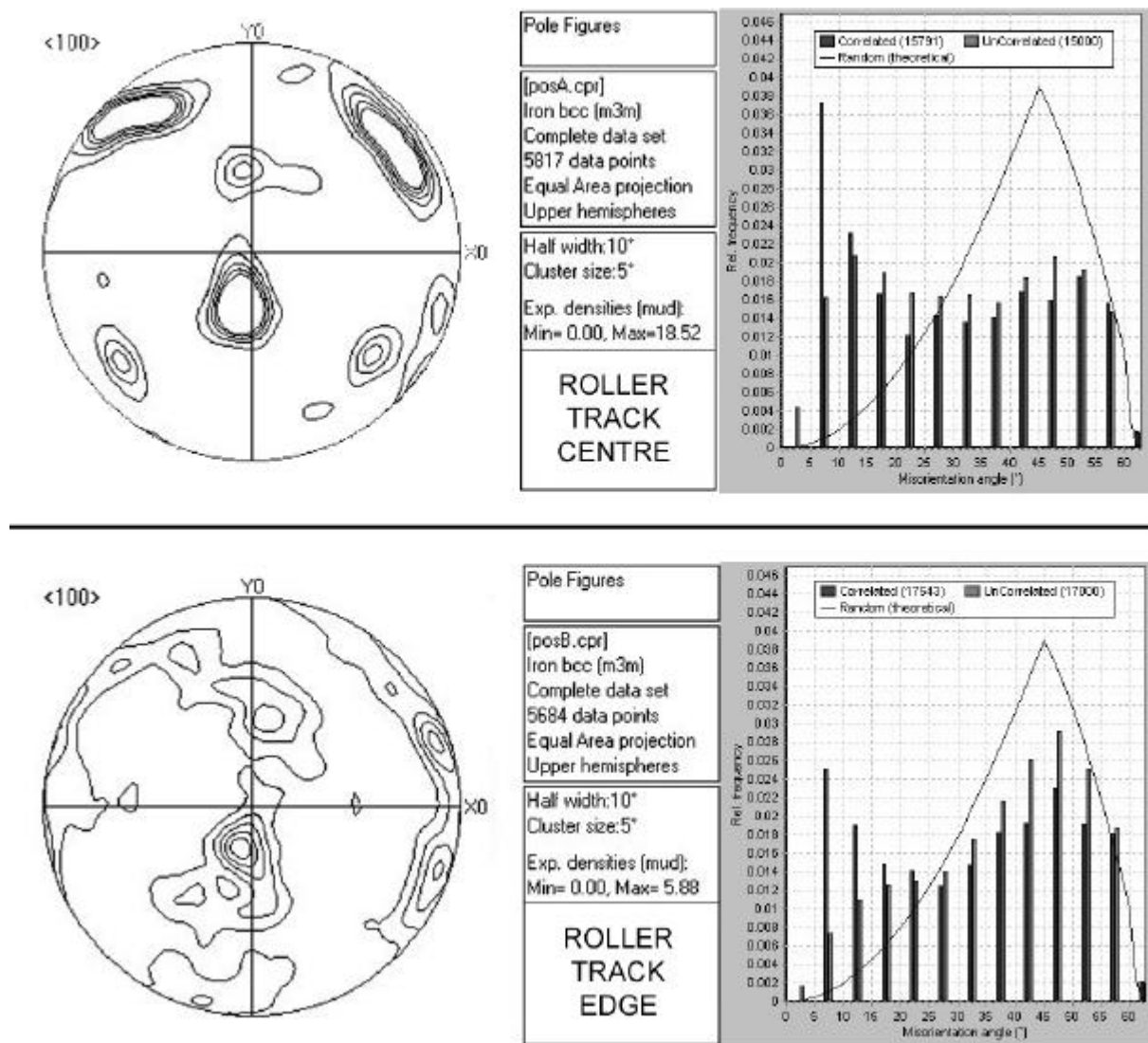


Figure 25

$\langle 100 \rangle$ pole figures and misorientation angle distributions from areas at the centre and edge of the flow forming roller tracks just below the outer surface of tube W7.

The plane of the page is parallel to the tapered sample surface and is at an angle of approximately 3° to a plane tangential to the tube surface. The Y direction is parallel to the tube hoop direction and the X direction parallel to the tube axis. The stronger pole figure shows a texture with $\langle 100 \rangle$ normal to the tube surface and $\langle 110 \rangle$ parallel to the tube axis and hoop directions. The deviation of the main spot from the figure centre is due to the 3°

difference in tube surface and sample surface. There is evidence of some fibrous rotation around this central axis and the figure is altogether similar to those found in cold flow formed tubes.^[12] There is also a weaker texture with $\langle 111 \rangle$ normal to the tube surface and $\langle 110 \rangle$ parallel to the tube axis. The pole figure from the roller track edge is much weaker and less well defined. Although there are similarities with the figure from the track centre, the primary texture is barely discernable and the secondary texture seen at the track centre is not apparent at all. The misorientation angle distribution histograms also show differences between the two areas. It can be seen that at the roller track centres there is a slightly higher concentration of low angle grain boundaries, particularly between neighbouring (Correlated) grains, whereas at the track edges the misorientation angle distribution approaches the theoretical random distribution.

It would appear that the deformation level at the surface of the tube along the centres of the flow forming roller tracks is significantly higher than that at the track edges. The texture at the track centres is stronger and there is a higher concentration of low-angle or subgrain boundaries, implying higher dislocation concentrations. This is not unreasonable as the geometry of the flow forming rollers is such that the diameter of the rollers at the leading and trailing edges is less than that at the centre-line of the roller face so that the roller bears much more heavily on the tube along the track centres than it does at the edges. It may be that the reason that the material at the track centres recrystallises so much more readily than that at the track edges relates to a greater local driving force for recrystallisation.

CONCLUSIONS

- Powder particle size has no effect on short-term oxidation behaviour. However, a large range of particle sizes in a powder sample can lead to close packing of the powder particles and the formation of a 'crust' on the surface that substantially protects powder within the sample from further oxidation.
- The presence of aluminium depleted regions (ADRs) within powder particles leads to the formation of defective, rapidly-thickening scales, and reduces oxidation lifetime by 53% in long term cyclic oxidation of powders.
- Oxidation of ODS-Fe₃Al and PM2000 powders during high temperature annealing processes may be reduced by hydrogen purging of the canned powders, cold compaction of the powders or a combination of these two techniques prior to consolidation.
- Porosity is not seen to develop in ODS-Fe₃Al as it does in PM2000 after protracted high-temperature annealing. However, intrusions are observed to become detached from the bulk alloy by the growth of oxide particles and/or pores around the intrusion. Aluminium nitride particles grow within the bulk alloy due to ingress of atmospheric components through an unprotective alumina scale.
- The inclusion of vibrating baffles in fluidised beds of metallic powders gives some improvement to the separation characteristics. However, powder particle morphology is the prevalent factor in terms of segregation.
- A PM2000 alloy variant has been produced containing up to 1 wt.% of ODS-free Fe-powder. Early results suggest similarities between the recrystallisation behaviour of the ODS-free Fe variant and ODS Fe₃Al (variant PMWY2) containing fine-grained stringers.
- The recrystallisation behaviour of PM2000 is not readily affected by the recrystallisation of adjoining steel structures due to the disparate nature of the two alloys' recrystallisation parameters.

- Attempts to influence the recrystallisation behaviour of PM2000 by the addition of alumina particles have so far been unsuccessful. It is thought that the 0.86µm MPD particles are too small to be effective.
- Flow forming has been used to produce PM2000 alloy tubes with hoop-orientated grains at the outer surface and enhanced hoop creep strength.
- Grain structures formed in flow formed and secondary recrystallised PM2000 tubes are complex and are influenced by macroscopic variations in level of deformation-through-thickness. Variations in the level and nature of deformation at the outer surface of the tubes are spatially directly related to the tracks on the surface left by the flow forming rollers.

ACKNOWLEDGEMENT

This research was sponsored by the Advanced Research Materials (ARM) Programme, U.S. Department of Energy, Office of Fossil Energy under contract DE-AC05-96OR22464 managed by U.T.–Battelle, LLC.

REFERENCES

- [1] Jones, A.R. and Ritherdon, J.: *Proc. 13th Annual Conf. on Fossil Energy Materials*, Knoxville, Tennessee, May 11-13, 1999, Eds. Judkins et al. (ORNL 1999), paper 2.4
- [2] Ritherdon, J. and Jones, A.R.: *Proc. 14th Annual Conf. on Fossil Energy Materials*, Knoxville, Tennessee, April 25-27, 2000, Eds. Judkins et al. (ORNL 2000), paper 2.3
- [3] Ritherdon, J. and Jones, A.R.: *Proc. 15th Annual Conf. on Fossil Energy Materials*, Knoxville, Tennessee, April 30-May 2, 2001, Eds. Judkins et al., (ORNL, 2001)
- [4] Al-Badairy, H., Tatlock, G.J. and Bennett, M.J.: *Materials at High Temperatures* **17**(1-2) (2000), 101
- [5] Tolpygo, V.K. and Grabke, H.J. : *Oxidation of Metals* **41** (1994) 343
- [6] Ritherdon, J., Jones, A.R. and Wright, I.G.: *Proc. of the 2001 Powder Metallurgy Congress*, Nice, 22-24 October, 2001, Vol. 4, 133
- [7] Ritherdon, J., Jones, A.R. and Wright, I.G.: *Powder Metallurgy* **46**(3) (2003) 1
- [8] Chen, Y.L. and Jones, A.R.: *Metall. Mater. Trans. A.* **32A** (2001), 2077
- [9] Ritherdon, J. and Jones, A.R.: "Reduction in Defect Content of ODS Alloys" Report No. ORNL/Sub/98-SY382/03, June 2001
- [10] Ritherdon, J., Jones, A.R. and Wright, I.G.: "Recrystallisation - Fundamental Aspects and Relations to Deformation Microstructures", 2000, Risø National Laboratory, Denmark, 533
- [11] Humphreys, F.J.: *Acta Metallurgica* **25** (1977) 1323
- [12] Krieger Lassen, N.C.: "Recrystallisation - Fundamental Aspects and Relations to Deformation Microstructures", 2000, Risø National Laboratory, Denmark, 393